

Dynamic modeling and scaling of nanostructure formation in the lithographically induced self-assembly and self-construction

Lin Wu^{a)} and Stephen Y. Chou

NanoStructure Laboratory, Department of Electrical Engineering, Princeton University, Princeton, New Jersey 08544

(Received 6 August 2002; accepted 13 March 2003)

We numerically studied the dynamical formation process and the scaling of the nanostructures in the lithographically induced self-assembly and self-construction of thin polymer films. Our studies show that the period of the self-assembled pillars depends on the ratio between the surface tension force and the electrostatic force. The viscosity of the polymer has no effect on the final pillar shape. When the feature width of the mold is comparable to or smaller than the most unstable disturbance wavelength of the system, the initially self-assembled pillars will merge to form a self-constructed mesa. © 2003 American Institute of Physics. [DOI: 10.1063/1.1572963]

Lithographically induced self-assembly (LISA),^{1,2} is an electrohydrodynamic instability process, in which an initially flat thin polymer film self-assembles into well organized periodic pillar arrays that bridge the lower substrate and the upper flat mask [Fig. 1(a)]. Lithographically induced self-construction (LISC),³ is a similar process. But LISC forms a polymer mesa under the mask, which is a positive replica of the protruding mask pattern [Fig. 1(b)], instead of pillar arrays.

In a typical LISA experiment [Fig. 1(a)], a mask is separated from a thin polymer film by a gap using spacers. Underneath the mask, an electrical field, which is either internally generated by the contact potentials or externally applied, causes a negative hydrodynamic pressure in the polymer film with a magnitude increasing with a decreasing mask-polymer spacing. The electrical force overcomes the surface tension force and pulls the interface upwards to form pillars. A well-defined periodicity of the pillar arrays is setup by the balance between the size refining process driven by the electrostatic force and the size coarsening process driven by the surface tension force.

The previous theoretical studies of the LISA problem were based on linear theories.⁴⁻⁶ According to these studies, the system is always unstable subject to infinitesimal disturbance. The driving force of the instability is the electrostatic force and the stabilizing force is the surface tension force. But the scaling mechanism that decides the pillar size is still not fully understood and the LISC formation process cannot be explained by the previous theories. In this letter we address these unanswered questions through linear instability analysis and a fully nonlinear numerical simulation of the LISA and LISC.

We first formulate the nonlinear equation that governs the LISA and the LISC process. In our model we ignore the air motion and assume the polymer flow to be an incompressible Newtonian flow with a low Reynolds number. Under a lubrication assumption, the horizontal Poiseuille volume flow rate is obtained as

$$q_x = \int_0^h u dz = -\frac{1}{3\mu} \frac{\partial p}{\partial x} h^3, \quad (1)$$

where u is the velocity in the x direction, h is the film thickness, and μ is the polymer dynamic viscosity. The pressure p is uniform across the film thickness and is decided by a normal stress balance at the air-polymer interface

$$p = p_0 - \sigma h_{xx} / (1 + h_x^2)^{3/2} + p_e + p_{\text{dis}}, \quad (2)$$

where p_0 is the ambient air pressure, σ is the surface tension coefficient, h_x and h_{xx} are the first and second order derivatives of h with respect to x , respectively. $p_e = -\varepsilon_0 \varepsilon_p (\varepsilon_p - 1) U^2 / [\varepsilon_p d - (\varepsilon_p - 1) h]^2$ is an electrostatic pressure exerted on the interface by the interaction of the electrical field with the polarization charges at the interface.⁴ In the formula for p_e , ε_0 and ε_p are the dielectrical constants of the air and the polymer, respectively, U is the voltage between the mold and the substrate, d is the mask-substrate spacing. The disjoining pressure $p_{\text{dis}} = A_2/h^2 - A_3/h^3$ is a result of the intermolecular forces exerted on the thin film,⁷ in which A_2 is a constant of the order 10^{-12} N and A_3 is a constant of the order 10^{-19} N m.

A mass balance gives the dimensionless governing equation for the air-polymer interface profile

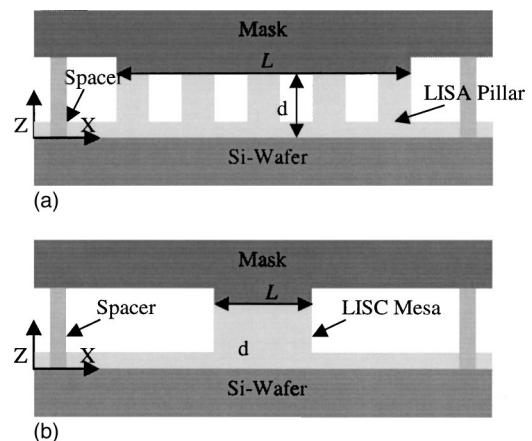


FIG. 1. Diagram of the experimental setup: (a) LISA and (b) LISC.

^{a)}Electronic mail: lwu@ee.princeton.edu

$$\frac{\partial H}{\partial T} + \frac{\partial}{\partial X} \left(H^3 \frac{\partial P}{\partial X} \right) = 0, \quad (3)$$

where H is the dimensionless film thickness normalized by the initial film thickness h_0 , X is the dimensionless horizontal coordinate normalized by the width of the mask L . $P = \alpha H_{XX} / (1 + R_l H_X^2)^{3/2} + 1 / [\epsilon_p D - (\epsilon_p - 1) H]^2 - \beta_2 / H^2 + \beta_3 / H^3$ is the normalized pressure. $\alpha = \sigma h_0^3 / U^2 L^2 \epsilon_0 \epsilon_p (\epsilon_p - 1)$ is a ratio between the surface tension force and the electrostatic force. $R_l = h_0 / L$ is a length scale ratio. $D = d / h_0$ is the normalized mask/substrate distance. $\beta_2 = A_2 / U^2 \epsilon_0 \epsilon_p (\epsilon_p - 1)$ and $\beta_3 = A_3 / h_0 U^2 \epsilon_0 \epsilon_p (\epsilon_p - 1)$ are ratios between the dispersion forces and the electrostatic force. T is the dimensionless time normalized by $3 \mu L^2 / U^2 \epsilon_0 \epsilon_p (\epsilon_p - 1)$. Since the polymer viscosity only participates in scaling the time, it has no effect on the final pillar shape. Larger viscosity requires longer time to form complete pillars.

A linear instability analysis of Eq. (3) gives the most unstable wavelength of the system

$$\lambda_m = 2 \pi \sqrt{\frac{2 \alpha (\epsilon_p D - \epsilon_p + 1)^3}{2 (\epsilon_p - 1) + (2 \beta_2 - 3 \beta_3) (\epsilon_p D - \epsilon_p + 1)^3}}. \quad (4)$$

The system is always unstable. The driving force of the instability is the electrostatic force. The surface tension force stabilizes the system. The dispersion force with a β_2 constant destabilizes the system when $\beta_2 > 0$, otherwise it stabilizes the system. The dispersion force with a β_3 constant stabilizes the system when $\beta_3 > 0$, otherwise it destabilizes the system. Equation (4) shows that a smaller ratio between the surface tension force and the electrostatic force, corresponding to smaller α and D , produces a smaller most unstable wavelength (or the horizontal feature size of the formed structure).

Equation (3) is solved by an implicit Crank–Nicolson finite difference numerical scheme.⁸ Within each iteration the linearized sparse matrix is inverted by a preconditioned bi-conjugate gradient method.⁹ At the two horizontal ends, we apply periodic boundary conditions. At the mask surface, we apply nonpenetration boundary condition.

We first compare our simulation results with the published experimental data.¹ In Fig. 2(a), h_0 is 95 nm, d is 260 nm, and L is 50 μm . The dielectrical constant of poly(methylmethacrylate) (PMMA) polymer is 3.6. We do not know the exact value of the voltage being internally built. But if we choose the ratio σ / U^2 to be 2.175 E-4, then the code predicts 15 pillar periods [Fig. 2(a)], which matches the experimental result shown in the inset (the inset only shows half of the pillars).¹ The simulation indicates that there is a small hump in between two pillars. These small humps are observable in the experimental picture. At temperature 150 °C, the surface tension coefficient σ for PMMA is 31 mN/m. The chosen ratio of σ / U^2 corresponds to a voltage of 11.9 V, which is a reasonable value under the experimental condition. Equation (4) predicts 13.8 periods using the same parameters. In Fig. 2(b) we fix all other parameters, but change d to 280 nm, and shrink L to 14 μm . The code predicts four periods, which exactly matches the experimental result shown in the inset.¹ Equation (4) predicts 3.34 pe-

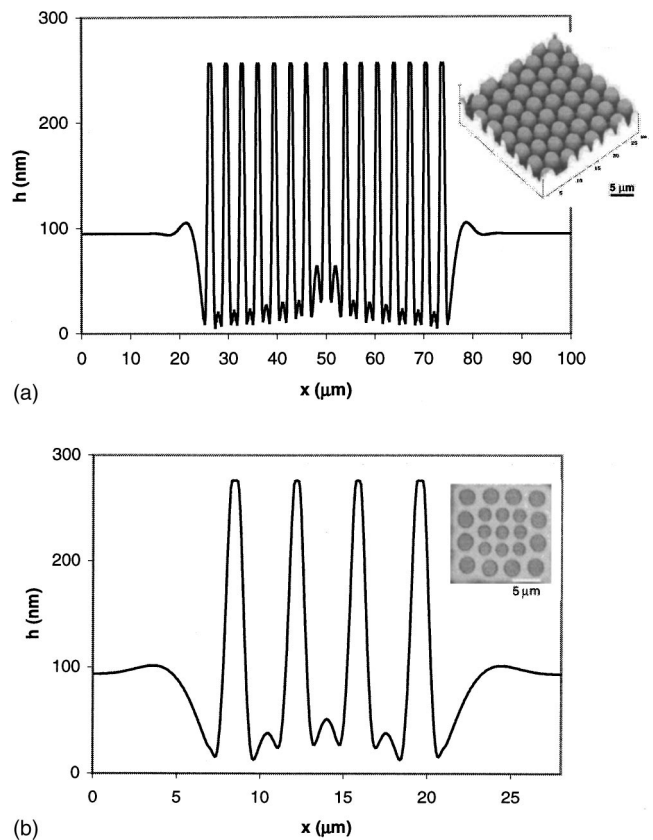


FIG. 2. Simulated LISA pillars: (a) d is 260 nm, l is 50 μm ; (b) d is 280 nm, l is 14 μm . In both cases, h_0 is 95 nm, σ is 31 mN/m, and U is 11.9 V. The insets are the corresponding LISA pictures from experiments under similar condition [inset in (a) only shows half of the LISA domain] (see Ref. 1).

riods. In both cases Eq. (4) gives a close estimation to the pillar period when the mask pattern size L is much larger than the most unstable wavelength.

Next we investigate the dynamic behavior of the LISC mesa formation. In Fig. 3, h_0 is 95 nm, d is 190 nm, and L is 0.5 μm . The magnitude of the ratio σ / U^2 is still fixed as 2.175 E-4. Figure 3 clearly shows that two LISA pillars are initially formed under the two mask edges (the dashed lines mark the mold edges). The electrostatic force tends to push

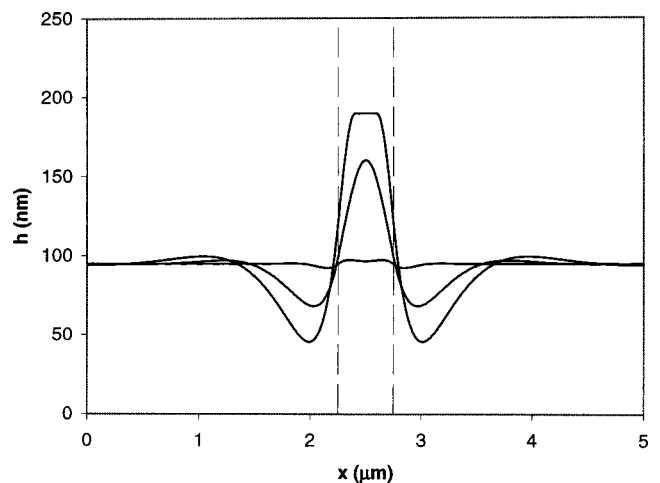


FIG. 3. Two initially formed LISA pillars merge into one before they reach the mask. A LISC mesa is formed consequently. The dashed lines mark the mold edges.

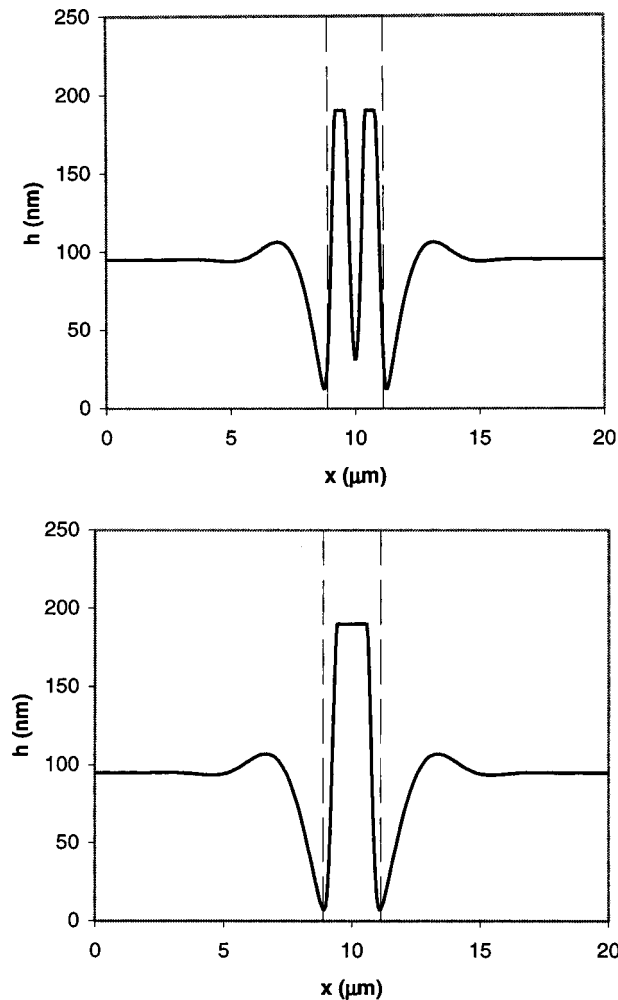


FIG. 4. Two LISA pillars reach the mask as two distinct pillars and then merge into a single LISC mesa. The dashed lines mark the mold edges.

the two pillars together as it pulls them upwards. The surface tension force also pulls the meniscus in between the two pillars upwards. As a result, the two pillars gradually merge together before they reach the top. After the single pillar reaches the mask, it spreads into a LISC mesa. Figure 4 shows another LISC formation mechanism. If we keep all other parameters the same as in Fig. 3, but increase L to $2.25 \mu\text{m}$, the two pillars initially formed under the mask edges reach the mask as two distinct pillars [Fig. 4(a)]. Then they merge into a single LISC mesa through spreading at the mask surface [Fig. 4(b)]. As a result, the mold width plays an important roll in deciding if LISA pillars or LISC mesa will form under the mask. Figure 5 plots the LISA/LISC boundary. In Fig. 5, except L , all other geometrical parameters are the same as in Fig. 3. Different σ/U^2 values are used to achieve different most unstable wavelengths from Eq. (4). For a particular σ/U^2 , L is changed to find the LISA/LISC boundary. The LISA/LISC boundary is represented by the curve with solid circles. In the region above this curve, the LISA pillars are observed to be stable, they will not merge into a LISC mesa later. Below the curve, the two initially formed LISA pillars gradually merge into a LISC mesa. The

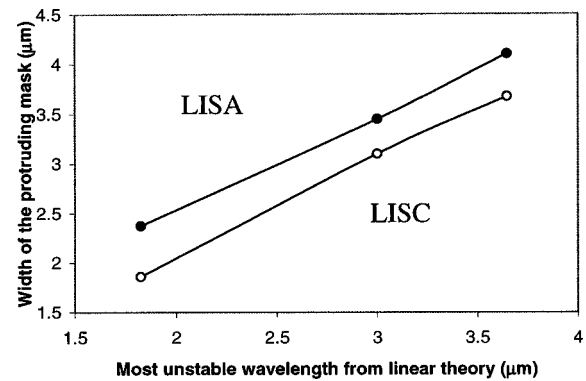


FIG. 5. The LISA/LISC boundary.

curve with open circles is the boundary, below which the initially formed two LISA pillars merge into one before they reach the mask and then they spread into a LISC mesa. Within the region between the two curves, the initially formed two pillars reach the mask as two distinct pillars, but they merge into one LISC mesa later. Figure 5 indicates that if L is comparable to or smaller than the most unstable wavelength, the formed polymer structure will be the LISC mesa instead of the LISA pillars. In our current simulation we do not take the chemical property of the mask surface into account. If the surface energy of the top plate is high, it is possible to form LISC mesa with a size much larger than the most unstable wavelength.

In summary our analysis indicates that submicrometer scale LISA pillars are achievable when the surface tension/electrical force ratio is small, which corresponds to a larger voltage, a smaller surface tension coefficient, a thinner initial polymer film thickness, and a smaller ratio between the mask-substrate separation and the initial film thickness. Final pillar size depends on the relative magnitude of the surface tension force and the electrical force instead of their absolute values. LISC is well suited to form submicrometer size structures, because if the mold feature width is smaller than the most unstable disturbance wavelength of the system, which is normally micrometer sized, LISC mesa will form. For LISA it is more difficult to achieve smaller pillars. For LISC it is more difficult to achieve larger mesa.

This work was supported in part by DARPA.

- ¹S. Y. Chou and L. Zhuang, *J. Vac. Sci. Technol. B* **17**, 3197 (1999).
- ²E. Schaffer, T. Thurn-Albrecht, T. P. Russell, and U. Steiner, *Nature (London)* **403**, 874 (2000).
- ³S. Y. Chou, L. Zhuang, and L. Guo, *Appl. Phys. Lett.* **75**, 1004 (1999).
- ⁴E. Schaffer, T. Thurn-Albrecht, T. P. Russell, and U. Steiner, *Europhys. Lett.* **53**, 518 (2001).
- ⁵Z. Suo and J. Liang, *Appl. Phys. Lett.* **78**, 3971 (2001).
- ⁶L. F. Pease and W. B. Russel, *J. Non-Newtonian Fluid Mech.* **102**, 233 (2002).
- ⁷G. F. Teletzke, H. T. Davis, and L. E. Scriven, *Rev. Phys. Appl.* **23**, 989 (1988).
- ⁸W. F. Ames, *Numerical Methods for Partial Differential Equations*, 2nd ed. (Academic, New York, 1977).
- ⁹W. H. Press, S. A. Teukolsky, W. T. Vetterling, and B. P. Flannery, *Numerical Recipes in Fortran 77* (Cambridge University Press, Cambridge, 1992).